

Article

Formation of Carbonate Nanoglobules by a Mixed Natural Culture under Hypersaline Conditions

Nurgul Balci * and Cansu Demirel

Department of Geological Engineering, Istanbul Technical University (ITU), Ayazaga Campus, 34469 Maslak, Istanbul, Turkey; cns-demirel@hotmail.com

* Correspondence: ncelik@itu.edu.tr; Tel.: +90-212-285-6118

Academic Editor: Juan Diego Rodriguez-Blanco

Received: 4 September 2016; Accepted: 2 November 2016; Published: 11 November 2016

Abstract: The present study demonstrated formation of Ca and P rich nanoglobules by a mixed natural halophilic population enriched from hypersaline lake sediments in laboratory culture experiments. Nanoglobules consisting of complex mixture of Ca, P, O, and C with minor amount of Mg occurred in the external envelop of bacterial cell in the first week of incubation at various Mg^{+2}/Ca^{+2} ratios and salinity at 30 °C. Unlike the control experiments (e.g., non-viable cells and without cells), later aggregation and transformation of nanoglobules caused the precipitation of calcium and/or magnesium carbonates in variable amount depending on the Mg^{+2}/Ca^{+2} ratios of the medium after 37 days of incubation. By showing the nucleation of carbonates on bacterial nanoglobules closely associated with the cell surfaces of mixed natural population this study emphasis that formation of nanoglobules may not be specific to a microbial strain or to activity of a particular microbial group. Formation of carbonate nanoglobules under various conditions (e.g., Mg^{+2}/Ca^{+2} ratios, salinity) with the same halophilic culture suggest that the although metabolic activity of bacteria have an influence on formation of nanoglobules the mineralogy of nanoglobules may be controlled by the physicochemical conditions of the precipitation solution and the rate of mineral precipitation.

Keywords: nanoglobules; halophilic bacteria; Lake Acıgöl; carbonates

1. Introduction

Tracing microbial activity in the geologic records primarily rely on our knowledge obtained from the recent laboratory experiments and field observations in geologically diverse environments. The finding evidence for existence of microorganism in the geologic record, particularly for carbonate, stimulate researches to develop new proxies for identifying microbial fingerprints as well as their role in carbonate precipitation under various geochemical conditions. Much attention has been put on carbonate minerals considered as indicator of biosignatures for extraterrestrial life and of paleo environmental conditions in diverse environments [1–7]. By regulating C, N and P, microorganisms cause precipitating a wide range of minerals such as carbonates, oxides and phosphates [8–10]. It is now widely accepted that formation of carbonates in marine (e.g., foraminiferal calcite, and corals) and fresh water environments (e.g., surface fresh water deposits, and tufas) is influenced by microbial activity. Numerous laboratory experiments and field studies have been carried out to elucidate the role of microorganism in precipitation of carbonate minerals [5–7,11–13]. Precipitation of phosphate is often related to carbonates and calcium phosphate minerals are considered an important sink for phosphorus in various environments (e.g., marine, and microbialites). Therefore, geochemical cycles of P and Ca exert significant control on carbonate precipitation processes in particularly organic rich environments. A diverse microbial population is generally involved in carbonate and phosphate precipitation in various natural settings. Nevertheless, our knowledge about the exact role played by bacteria during

biomineralization of carbonates and phosphates is still missing in many cases. It is still under debate if mineralization occurs due to side effect of metabolism (e.g., biologically induced) or an intentional effect of microorganism to benefit from their environment. Various mechanisms have been proposed for bacterial precipitation of carbonates: One mechanism, termed as biologically induced or biotically induced precipitation, suggest that precipitation of minerals occurs as a result of interactions between metabolic activity of bacteria and the environment [8,14,15]. Recent experimental studies suggest that biotically induced precipitation may include two fundamentally different processes: (1) metabolic activities employed by bacteria within its particular redox environment mediate pH and pCO₂ in a way that an increase in saturation state of a particular mineral phase occur and thereby indirectly favoring precipitation of a particular mineral phase called as microbially influenced carbonate precipitation (MICP); and (2) bacteria can act as a catalyzer to lower a kinetic barrier which inhibit the precipitation of the mineral from a solution already supersaturated with respect to that mineral, microbially catalyzed carbonate precipitation (MCCP) [16]. Although both types of precipitation can be operative in biotically induced precipitation, in most cases it is difficult to distinguish their products. Another long standing question is how and where nucleation processes start. The close spatial relationship between microorganism and carbonate minerals in natural and laboratory conditions suggest that the bacterial surface may act as a nucleation site via a secreted exopolymeric substances (EPS) or specific chemical groups although the exact mechanism of nucleation is not known [5,17–20]. Formation of nanoglobules on the surface of bacteria are reported under various experimental conditions (e.g., oxic, anoxic, pH, temperature, etc.) [14,21,22] and proposed as a first step for microbial carbonate precipitation by sulfate reducing bacteria [21] and cyanobacteria [23,24]. Carbonate nanocrystals and nanoglobules on the surface of pure halophilic bacterial cell have also been shown by Rivadeneyra et al. [14,15] and Sánchez-Román et al. [22]. Although these studies demonstrated microbially mediated nanoglobule formation and later precipitation of carbonate minerals, the exact mechanism of nucleation remain unsolved. Additionally, how abiotic factors such as salt concentration, ionic composition of the medium (e.g., Mg⁺²/Ca⁺² ratio), fluid chemistry and viscosity effect on nucleation processes is not exactly known. It is still a question whether a metabolic diversity is involved in formation of nanoglobules and to date there are no such experimental studies fully exploring these. Most of our knowledge on bacterial nanoglobules came from experiments carried out with pure strains [14,21,22].

A diverse microbial consortium rather than a single microorganism is commonly involved in carbonate and phosphate precipitation in natural environments [5,9,25,26]. In this respect, saline lakes and their halophilic microorganisms give an opportunity to study effect of abiotic factors on bacterial nanoglobules formation and biomineralization processes under natural conditions. A better understanding of bio precipitation processes in these lakes may provide crucial information regarding elucidating precipitation mechanism of carbonates and the effect of environmental conditions on the processes in modern and geological past as well as search for life in extraterrestrial environments.

This study was conducted to examine: (1) if a mix natural population of chemoorganotrophic halophiles enriched from recent sediments of a hypersaline lake is able to precipitate carbonates; and (2) if the nucleation of carbonates on bacterial nanoglobules demonstrated for pure strain culture experiments would occur in mix halophiles consortium under various physicochemical conditions (e.g., salinity and Mg⁺²/Ca⁺² ratios). The current study represents a first sequence of experimental results to systematically evaluate bacterial nanoglobule formation under hypersaline conditions and may provide insights into microbial carbonate precipitation process in geologically diverse environments.

2. Materials and Methods

2.1. Site Description

Lake Acıgöl, located in southwestern Turkey with an elevation of 836 m above sea level, is one of the saltiest lakes in Turkey (Figure 1). The lake's drainage basin, covering ca. 1292 km², is a

closed basin in a tectonically active rift region. The playa lake has a surface area of 60 km² with a maximum depth of 2–3 m [27]. The climate in the region where the lake is located is semiarid with precipitation of 368–392 mm and an annual temperature 13 °C (General Directorate of State Hydraulic Works, 2008). The water level and depth of the lake changes seasonally, with maxima in March and minima in August. Changes in the lake's water level create dry muds and brine pools that often contain salt precipitation with a unique microbial community [9]. Lake Acıgöl brines are predominantly Na-Cl-SO₄ type with Mg⁺²/Ca⁺² ratios ranging from 5 to 9 depending on the season (Table 1). Formation of various authigenic minerals such as calcite with lesser amounts of dolomite, aragonite, gypsum crystals, low magnesian calcite, huntite and hydromagnesite are reported [9,27,28]. In addition, microbial mats along the shoreline of the lake where formation of recent exotic carbonate minerals (e.g., huntite, nahcolite, kutnohorite, and dypingite) occur is reported by Balci et al. [9].

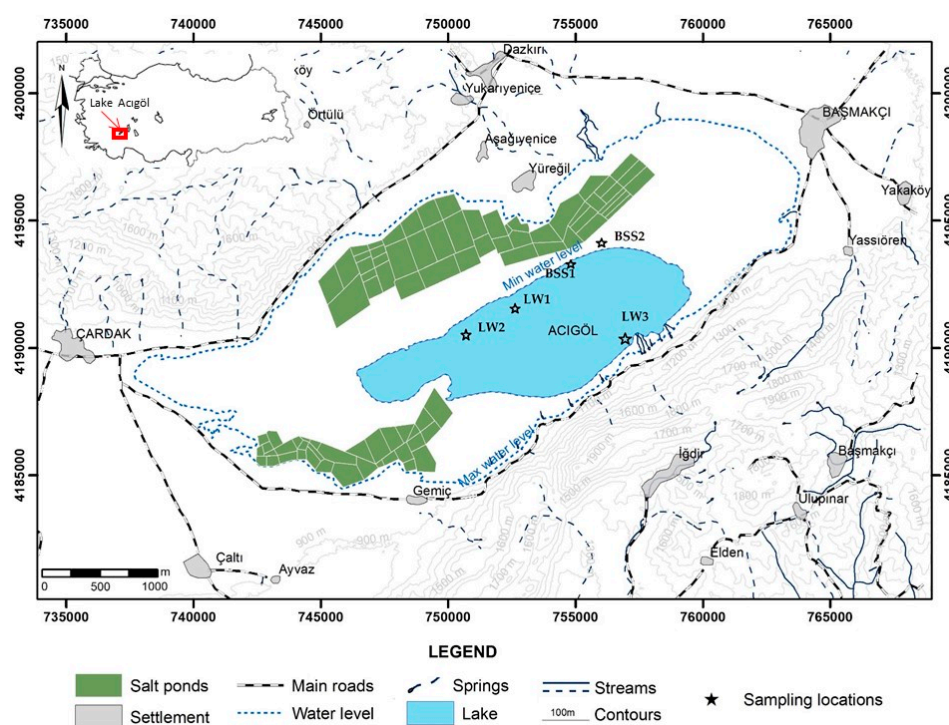


Figure 1. Location of the study area and sampling points in Lake Acıgöl, SW Turkey.

Table 1. Physico-chemical characteristics of the lake and the saltern ponds water overlying the sampled sediments.

Sample	LW ₁ ^a	LW ₂	LW ₃	BSS ₁ ^b	BSS ₂
pH	8.2	8.5	8.6	8.3	8.7
T (°C)	22	-	29	24	32
EC (µS/cm)	62,100	58,200	85,200	95,230	123,532
Cl ⁻ (mmol/L)	1131.4	672	1214.2	4071.4	1578.5
SO ₄ ²⁻ (mmol/L)	100	89.58	130.2	820.9	891.6
Mg ⁺² (mmol/L)	138.5	57.3	123.3	120.4	135.4
Na ⁺ (mmol/L)	963.6	511.3	1165	1361.9	840.9
K ⁺ (mmol/L)	22.1	13.6	24.6	11.5	22.82
Ca ⁺² (mmol/L)	17.25	14	30	13.25	18.7
Salinity (g/L)	70	n.d.	75	n.d.	82
CO ₃ ²⁻ (mmol/L)	-	1.8	-	-	-
HCO ₃ ⁻ (mmol/L)	n.d.	12.4	19.2	n.d.	n.d.

^a Lake water; ^b saltern pond water; n.d not determined.

2.2. Sample Site and Enrichment of Halophilic Culture

Mixed halophilic culture were enriched from hypersaline Lake Acıgöl's surface sediments. A variety of sediment samples were collected from the different parts of the lake (Table 1): brine soak sediment containing salt precipitation (BSS) along the shoreline of the lake and recent sediment samples from 15 to 30 cm depth in the lake (LW) (Figure 1). The respective sediment samples were taken in triplicate from each sampling point with a sterile spatula and placed into a sterile centrifuge tube and kept at 4 °C until further processes. The triplicate samples were homogenized in a microbiological cabinet under sterile conditions. The mixed enriched halophilic culture was prepared following the methods of Schneegurt, 2012 [29]. About 10 g of homogenized sediment was placed into 90 mL of medium containing 0.5 g/L of sodium acetate, 0.5 g/L of yeast extract, 0.5 g/L of casamino acids, 0.5 g/L of sodium thiosulfate, and 10% NaCl, supplemented with 60 mM magnesium and 10 mM calcium. Solution containing calcium and magnesium were filter-sterilized and added into the medium. The pH was adjusted to 7.2 with 1 M sterile KOH. The sample was incubated at 30 °C for 7 days while being shaken at 180 rpm. Three subsequent culturing were performed before being used in the precipitation experiments. After three sub-culturing, genomic DNA was isolated from the enrichment cultures using the MoBio UltraClean™ Microbial DNA Isolation Kit (Catalogue No. 12224-50). Total bacterial DNA of enrichment was obtained by using the Fast DNA Spin Kit for Soil (Catalogue No. 6560-200, MPBio, Istanbul, Turkey) and DNA samples were eluted in 50 µL of TE buffer. The amount of DNA in the samples was estimated based on agarose gel (1%) electrophoresis and EZ Vision staining (Catalogue #N472-KIT).

Diversity of enrichment cultures was determined by the 16S rDNA UARR polymerase chain reaction (PCR). For this purpose, a pair of universal primers, namely pA-F (5'-AGAGTTTGATCCTGGCTCAG-3') and pH-R (5'-AAGGAGGTGATCCAGCCGCA-3'), was used for amplification. The obtained PCR products were visualized by agarose gel (1%) electrophoresis and purified by ROCHE, (Indianapolis, IN, USA)—High Pure PCR Product Purification Kit (Catalogue No. 11 732 668 001) according to the manufacturer's suggested protocol.

Purified PCR products carrying the 16S rDNA regions of microorganisms were cloned using the TOPO TA® Cloning Kit (Catalogue No. K4500-01, Invitrogen, MA, USA) and the 20 positive clones were selected according to the Blue-White Screening Method. White colonies ($n = 25$) were picked and inoculated in 15 mL of tubes containing 3 mL of LB broth and 3 µL of ampicillin stock solution (0.1 g/mL ampicillin). Then, they were incubated at 37 °C overnight with shaking. After incubation, plasmids were isolated by using the Roche High pure Plasmid Isolation Kit (Catalogue No. 1754785).

The sequencing was performed using the ABI Prism 3700 DNA Analyzer (Applied Biosystems, Waltham, MA, USA) automated sequencer at the Molecular Biology and Genetics Department at ITU. The results of sequence analysis were compared with the National Center of Biotechnology Information (NCBI) database using BLAST. Only sequences with high similarity (>95%) were accepted. Phylogenetic affiliation revealed that clones from the enrichment show 99% homology to *Idiomarina* sp. TBZ29, 98% *Idiomarina seosensis* strain CL-SP19, 98% homology to *Bacillus selenitireducens* strain M1S6-17, 98% homology to uncultured Bacterium clone TX4CB_04, 98% homology to *Virgibacillus marismortui* strain TPA3-3, 98% homology to *Halomonas saccharevitans* strain AJ275, 98% homology to *Salinicoccus roseus* strain DSM 5351, 98% homology to *Halomonas alimentaria* strain L7B, 98% homology to uncultured Bacterium clone A5-10.1, 97% homology to *Planococcus maritimus* isolate LLQ, and 99% homology to *Planococcus rifietoensis* strain M8.

2.3. Culture Media

The enriched chemoheterotrophic halophilic culture was grown on the medium prepared with 1% (w/v) yeast extract, 0.5% (w/v) proteose-peptone, and 0.1% (w/v) glucose, supplemented with varying amount of NaCl to obtain 80 and 150 g/L salinity conditions before used in the carbonate precipitation experiments.

2.4. Carbonate Precipitation Experiments

The initial chemical compositions of the liquid culture media used for all the precipitation experiments is presented in Table 2. To prepare liquid culture media with different composition, 0.5% (*w/v*) proteose-peptone and 0.1% (*w/v*) glucose were added into 1 L distilled water (18 μ) and autoclaved at 121 °C for 30 min and left for cooling as a first step. After the cooling step filter sterilized solutions containing 1% (*w/v*) yeast extract, Mg⁺² (MgCl₂) and Ca⁺² (CaCl₂) were added into the liquid media to obtain desired Mg⁺²/Ca⁺² ratio (Table 2). As a final step pH of the medium was adjusted to 7.2 with sterile 0.1 M KOH. For each experiment 700 mL media with different salinity and Mg⁺²/Ca⁺² ratio and enriched halophilic culture (cell density = 10⁷ cells/mL) were placed into 1 L Erlenmeyer flask to provide sufficient headspace (Table 2). The experimental flasks were then loosely covered with a sterilized-cotton ball and thin aluminum foil to allow oxygen penetration into the flasks. Bacterial cell concentration of the inoculum was determined via optical density (O.D.) by using a spectrophotometer at 600 nm wavelength. Each experiment was done in duplicate. The liquid culture experiments designated as M (M1–M8) were aerobically incubated at 30 °C without stirring for 3, 5, 10 and 37 days and monitored at 4, 7, 10, 14, 21, 30 and 37 days for pH, Ca⁺² and Mg⁺² except M5 media. M5 media was incubated at 10 °C. Additionally, four petri dishes containing approximately 20 mL liquid media (M1–M8, except M5), 5 sterilized cover slips and enriched culture (1 mL) were set up to closely examine the involvement of bacteria into the precipitation processes. The glass cover slips were subsequently removed and further were subjected to morphological examination at 1, 3 and 5 days of incubation, respectively. The pH of the liquid culture was measured by a WTW330 probe while the precipitates were kept in the suspension. Calcium and magnesium concentrations were measured in the supernatants that were filtered with cellulose acetate filters (0.22 μ m Millipore, Frankfurt, Germany) by atomic absorption spectrophotometry (Perkin-Elmer 5100-AAS, Waltham, MA, USA) with an uncertainty of \pm 5%. Total nitrogen in the culture media was determined by Kjeldhal's method. Total phosphorus in the culture media is measured colorimetrically by the molybdate-blue/ascorbic acid method with color intensity measured at 880 nm with a UV-VIS spectrophotometer zeroed against a blank consisting of the extraction reagent [30]. Total organic carbon (TOC) and dissolved inorganic carbon (DIC) content of the medium were measured with a TOC Analyzer (Shimadzu, Tokyo, Japan) and monitored for 0, 10, 15, 37 days. Two different control experiments were performed with: uninoculated culture medium and culture medium inoculated with autoclaved bacterial cells (10⁷ cells/mL) (data is not presented).

Table 2. Ionic composition of the media used in the precipitation experiments.

Sample	Ca ⁺² (mmol/L)	Mg ⁺² (mmol/L)	Mg ⁺² /Ca ⁺²	Ca ⁺² + Mg ⁺² (total) (mmol/L)	pH	Salinity (g/L)	T (°C)
M1	23	2	0.1	25	7.2	80	30
M2	23	2	0.1	25	7.2	150	30
M3	13	13	1.0	26	7.2	80	30
M4	13	13	1.0	26	7.2	150	30
M5 *	10	40	4.0	50	7.2	80	10
M6	5	36	7.2	41	7.2	80	30
M7	5	36	7.2	41	7.2	150	30
M8	5	40	8.0	45	7.2	80	30

* Microbial growth did not occur.

2.5. Mineralogical and Morphological Examination of the Precipitates

To collect sub-samples from the liquid culture experiments after an incubation period of 3, 5 and 10 days, the flask was placed into the laminar flow (Faster Safe Fast212) under UV for 25 min to ensure sterile conditions. Following the sterilization step, 50 mL of the medium containing the precipitates were withdrawn and washed several times with distilled water to remove the cellular debris as well

as nutrition and air-dried at 37 °C. The precipitates from the culture experiments were analyzed with scanning electron microscopy (The Philips XL30 ESEM-FEG/EDAX system, Philips, Amsterdam, The Netherlands) equipped with an electron dispersive X-ray (EDX) detector when the microbial precipitates were visible under a petrographic microscope (x20). Morphological examination with SEM were also performed on the cover slides incubated for 3 and 5 days, respectively. The bulk precipitates obtained from the end of the experiments (37 days) cleaned following the above procedure and screened for mineral composition by X-ray diffraction, using a Philips diffractometer, with a CuK α radiation. The quantitative mineral composition of the bioliths was determined by applying Rietveld method [31].

2.6. Geochemical Study

The activity of dissolved species and degree of saturation in the experimental solution was determined using the PHREEQC V.2 hydrogeochemical modelling software [32]. The results of PHREEQC program were presented as saturation index (SI) for each predicted mineral phase where $SI = \log(IAP/Ksp)$. IAP is the ion activity product of dissolved mineral constituents in a solubility product (Ksp) for the mineral. $SI > 0$ indicate oversaturation with respect to the mineral whereas $SI < 0$ implies under saturation. The concentration of Mg^{+2} and Ca^{+2} used for all calculations was presented in Table 2. The values of Na^+ and Cl^- correspond to the addition of NaCl = 80 and 150 g/L and $PO_4^{3-} = 0.16$ g/L and $NH_4^+ = 1.4$ g/L values to the addition of proteose-peptone = 5 g/L and yeast extract = 10 g/L. Initial DIC value of each experiment was used as alkalinity for all calculations (Figure 4b). SI values were only calculated for initial chemical conditions of each experiment.

3. Results

3.1. Changes in Solution Chemistry during Precipitation

Figure 2 presents the pH evolution during the precipitation experiments in the presence of mixed halophilic culture. At the early stage of all liquid culture experiments (4–5 days), pH decreased to 6 or less than 6. The pH drop was even more pronounced in the experiments with M1 and M2 liquid culture with Mg^{+2}/Ca^{+2} ratio of 0.1 at 80 and 150 g/L salinity, respectively. Following a short fall, a significant pH rise ranging from 8.2 to 9 occurred in culture experiments (Figure 2). In general, a shorter time periods were required for a pH rise from 7.2 to 9.2 in the low salinity experiments (80 g/L) compared to those with the higher salinity (150 g/L). The highest pH value was obtained from M6 medium with 80 g/L salinity and Mg^{+2}/Ca^{+2} ratio of 7.2 at the end of 37-day incubation. An increase in both Mg^{+2} and Ca^{+2} concentration exceeding the starting concentration of both ions was determined at the early stage of experiments (Figure 3a–d). The initial increase in Mg^{+2} and particularly in Ca^{+2} concentration along with decrease in pH was attributed to possible dissolution of amorphous $Ca^{+2}-Mg^{+2}$ phases carried with the inoculum and/or attached to the cell wall. No changes in magnesium and calcium concentration and pH were detected in the control experiments (data is not presented). Unlike the control experiments (with the dead cell, without the cell), incubated under the same conditions with the culture mix natural halophilic culture precipitated carbonates and phosphate minerals in all experimental conditions except 10 °C (Table 3). Lack of microbial growth under low temperature could be related to high concentration of ions in the solution, and new experiments are currently underway to test this hypothesis. In general, time required for initial and wide spread precipitation increases with higher salinity. Precipitation of carbonates was also evident from decreasing concentration of magnesium and calcium from initial to final stages (Figure 3a–d). The percentages of total organic carbon consumption were in the range of between 42% and 66%, the lowest at M8 and the highest at M6 medium experiments (Figure 4a). In contrast, insignificant or slight changes were determined in dissolved inorganic carbon concentration over the course of the experiments (Figure 4b).

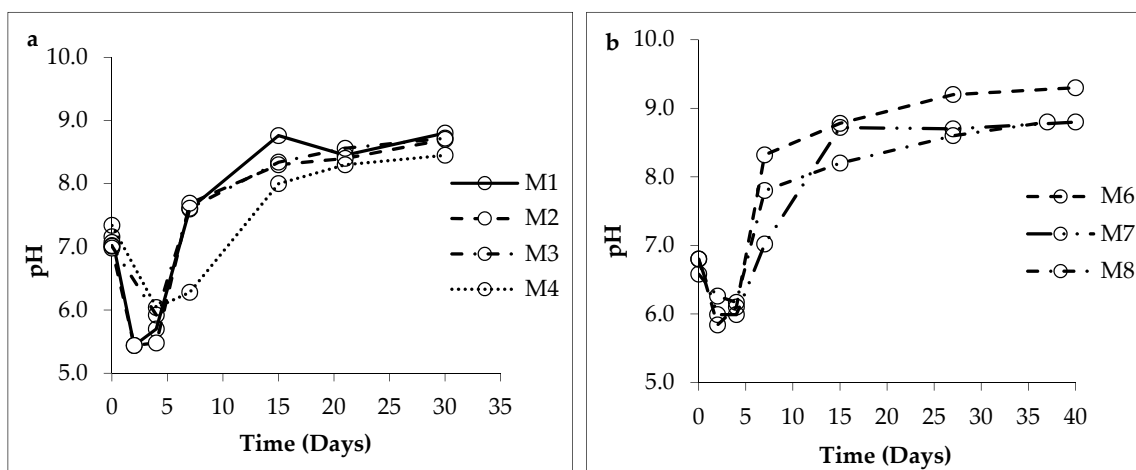


Figure 2. Evolution of pH during the precipitation experiments: (a) M1–M4; and (b) M6–M8 experiments.

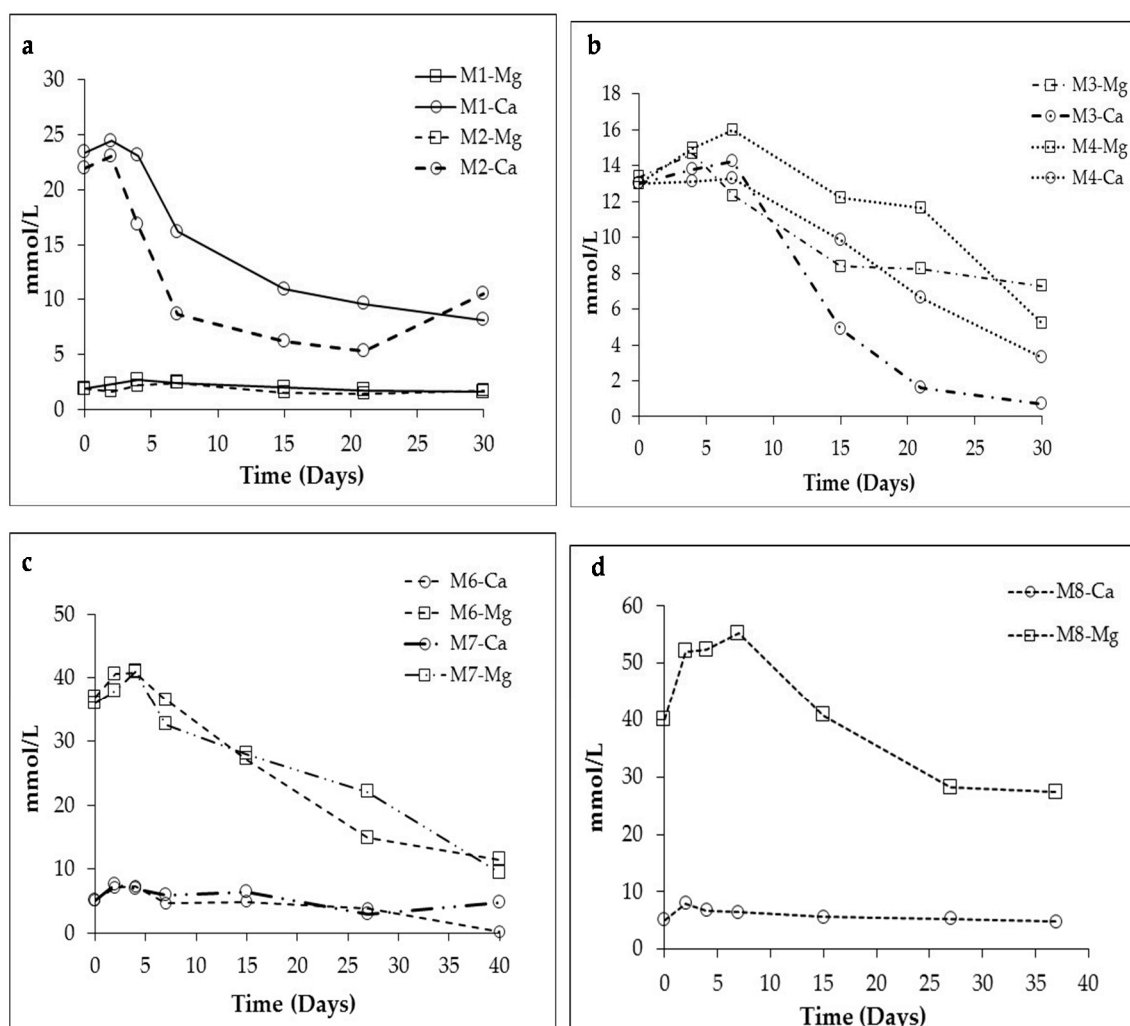
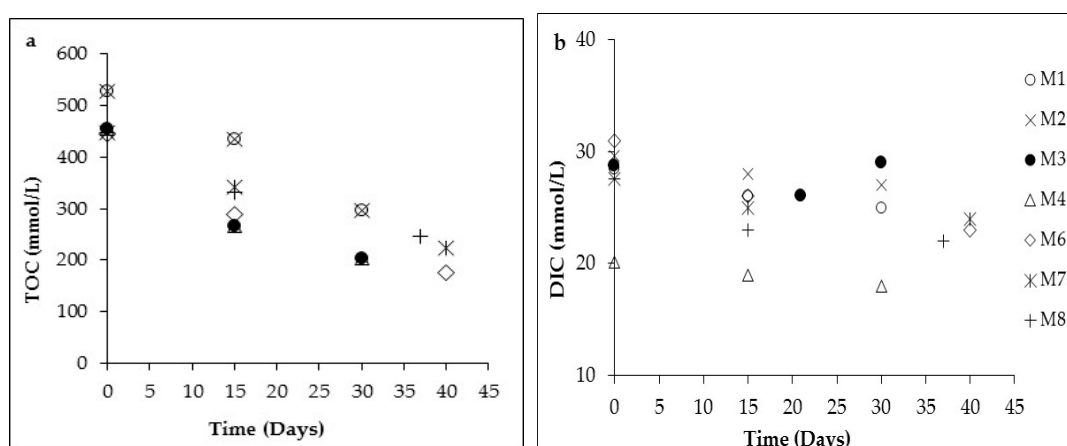


Figure 3. Evolution of Mg²⁺ and Ca²⁺ ions during the precipitation experiments: (a) M1–M2; (b) M3–M4; (c) M6–M7; (d) M8.

Table 3. Mineralogy of the bioliths derived from XRD analysis.

Experiment	Identified Minerals
M1	CAP (83 *)
M2	CAP (84)
M3	C (12), D (2), S (80.3)
M4	C (10), D (6), S (84)
M5	No data
M6	C (40.2), D (14.7), MHC (31.2), S (4.4)
M7	C (14), D (12), HM (33.7), S (36.7)
M8	MC (7.3), D (23), HM (38), S (21)

* Represents percentage of the mineral. CAP, Chlorapatite— $\text{Ca}_5(\text{PO}_4)_3\text{Cl}$; C, Calcite— CaCO_3 ; MHC, Monohydrocalcite— $\text{CaCO}_3 \cdot \text{H}_2\text{O}$; D, Dolomite— $\text{MgCa}(\text{CO}_3)_2$; HM, hydromagnesite— $\text{Mg}_5(\text{CO}_3)_4(\text{OH})_2 \cdot 4\text{H}_2\text{O}$; S, struvite— $(\text{NH}_4)\text{Mg}(\text{PO}_4) \cdot 6\text{H}_2\text{O}$; MC, Magnesian Calcite— $(\text{Ca},\text{Mg})\text{CO}_3$. Halite (NaCl) in M6, M7, M8 and amorphous phase in M1 and M2.

**Figure 4.** Evolution of total organic carbon (TOC) (a) and dissolved inorganic carbon (DIC) (b) during the precipitation experiments.

3.2. Mineralogy of the Bioliths

Table 3 shows the mineralogical and quantitative analysis of the bioliths according to the XRD data. Various amount of Ca and/or Mg carbonates was precipitated in variable amount depending on the $\text{Mg}^{+2}/\text{Ca}^{+2}$ ratios and salinity of the medium following 37 days of incubation. Calcite, dolomite, monohydrocalcite, magnesian calcite, hydromagnesite were identified carbonate minerals along with struvite and chlorapatite as phosphate minerals. In M3 through M8 experiments, carbonates and struvite co-precipitated in varying amount whereas in M1 and M2 media with $\text{Mg}^{+2}/\text{Ca}^{+2}$ ratio of 0.1 chlorapatite was the only mineral identified (Table 3). At $\text{Mg}^{+2}/\text{Ca}^{+2}$ ratio 1 with 8% salinity, calcite, dolomite and struvite were precipitated and the last was favored with increasing salinity. In media with $\text{Mg}^{+2}/\text{Ca}^{+2}$ molar ratio >1 , precipitations of struvite began first followed by carbonates, and struvite was the single phosphate mineral, whereas carbonate formed before struvite in the M3 and M4 media ($\text{Mg}^{+2}/\text{Ca}^{+2} = 1$). With increasing $\text{Mg}^{+2}/\text{Ca}^{+2}$ ratio calcite, dolomite, monohydrocalcite, hydromagnesite and magnesian calcite formed (M6, M7, M8) and predominate over struvite. At nearly the same $\text{Mg}^{+2}/\text{Ca}^{+2}$ molar ratios (M6 and M7) the media with increased salinity favor the formation of hydromagnesite and struvite. Interestingly, the high concentrations of Mg^{+2} in the culture media M6, M7 and M8 (Table 3) do not inhibit the formation of calcite.

3.3. Morphology and Texture of Bioliths

Examination of the precipitates under petrographic microscope revealed two types of mineral morphologies: struvite mineral with a large crystal (Figure 5b) and carbonates with spherical

(Figure 5a,b) dumbbell (Figure 5c) and small rounded aggregates (Figure 5d) developed around the bacterial colonies. SEM observations of the earliest precipitates indicated nanoglobules less than 300 nm in diameter with the irregular size and distribution in the close association with the bacterial surface after three and five days of incubations (Figure 6). These nanoglobules occurred attached to the surface of bacterial cells and in some cases they are embedded in EPS surrounding the cells (Figure 6a). Furthermore, in a close examination it can be easily observed that the surface of bacterial cells was completely covered by nanoglobules (Figure 6b,d) and nanoglobule aggregates (Figure 6c). Consistently, nucleation of nanoglobules in the intimate vicinity of the bacterial cell surface on the glass cover slides was evident after three and five days of incubation period (Figure 6e,f). SEM view of the cover slide after an incubation period of three days showed whitening on the polar ends of bacteria in addition to attachment of nanoglobules to the bacterial cell surface (Figure 6d). The size and distribution of nanoglobules are irregular and most of nanoglobules are in the size of 100 nm. Extensive formation of nanoglobules was particularly observed in the M6 and M7 experiments (Figure 6a,d). EDX analyses of these nanoglobules indicate Ca, P, C, O and minor amount of Mg^{+2} likely corresponds to a complex mixture of carbonate and phosphate phases which are precursory for later carbonate minerals (Figure 7). These nanoglobules (Figure 6d) appear to be rich in P and Ca even at high Mg^{+2}/Ca^{+2} ratio (Figure 7c).

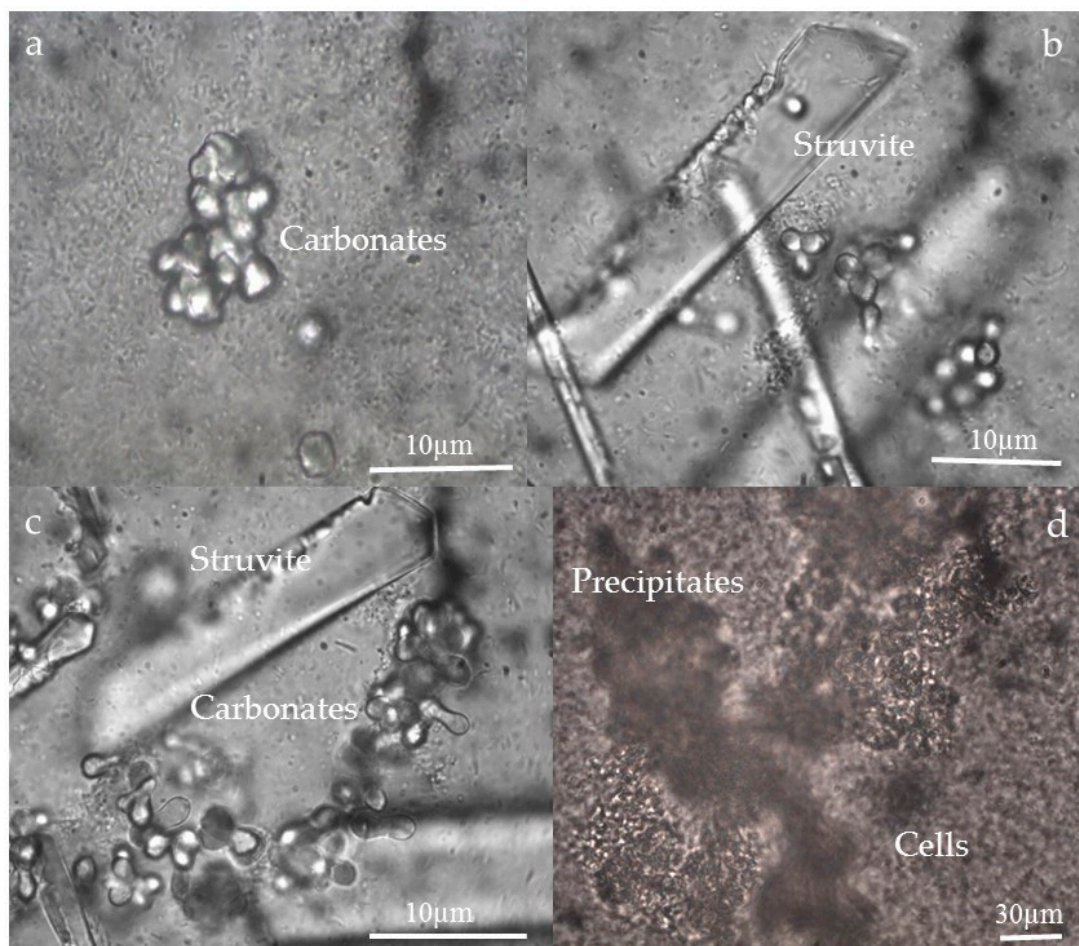


Figure 5. Light microscopic photographs of carbonate and struvite with a mix halophilic culture: (a,b) spherical calcite precipitate of different sizes formed (M3 and M6 experiments); (c) dumbbell-shaped dolomite precipitates (M6 and M8 experiments); and (d) small rounded aggregates around the bacterial colonies.

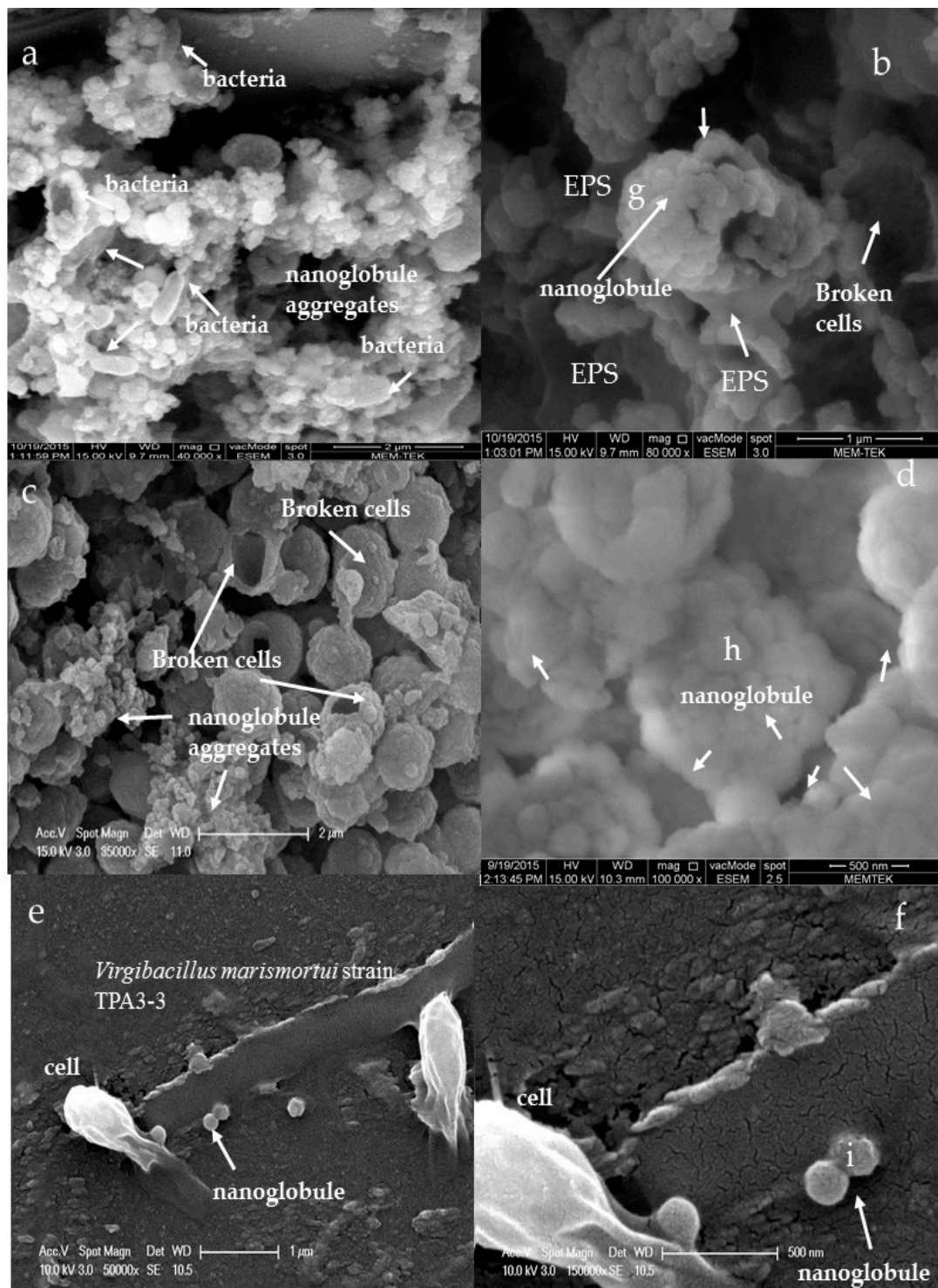


Figure 6. SEM photomicrographs of early precipitates in various experiments: (a,b) extensive formation of nanoglobules in the external envelop of cell and in EPS after three days incubation (M6 and M3 experiments, respectively); (c) nanoglobule and nanoglobules aggregates on cells after six days incubation (M4 experiment), note the nanoglobules delimiting ovoidal cell contours; (d) extensive formation of nanoglobule in the outer of bacterial cell after five days incubation (M4 experiment); (e) nanoglobules in the external envelop of *Virgibacillus marismortui* strain TPA3-3 after three days incubation (M3 experiment); and (f) a closer view of e.

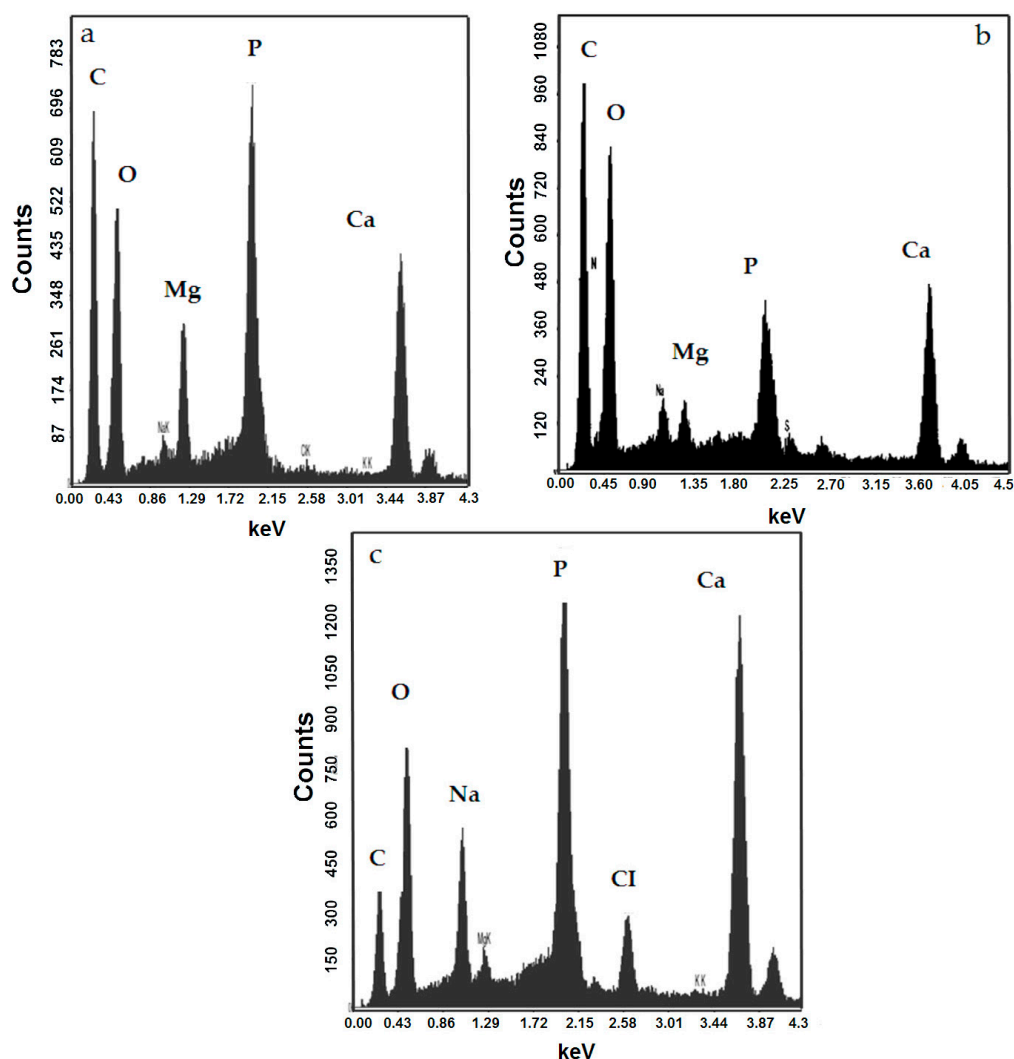


Figure 7. Energy dispersive (EDX) spectra of mineralized cells and nanoglobules indicated in Figure 6. (a) EDX spectra of g in Figure 6b; (b) EDX spectra of h in Figure 6d; (c) EDX spectra of i in Figure 6f.

SEM images of the bioliths obtained after 10-day incubation revealed spherulitic, ovoidal and dumbbell-shaped morphology (Figure 8). Nanoglobule aggregates were observed on the surface of dumbbells (Figure 8a,b). The surface of spherulites often contains nanoparticles with cells and nanoglobules (Figure 8c–f). EDX spectra indicate that these bioliths were composed of Ca, C, and O with lesser amount of P compared to the earliest precipitates (Figure 7). The Mg^{+2} content clearly increased in some of the bioliths (Figure 9c). EDX spectra suggest that the bioliths were composed of various Ca and Mg carbonates depending on the Mg^{+2}/Ca^{+2} ratios of medium. With extended incubation (37 days), spherulitic morphologies were dominant as mostly isolated spheres with smooth and rough surfaces with fibrous internal structure (Figure 9a). A close examination of fibrous internal structure revealed bacterial moulds (Figure 9c,d,f). Consistently, surface of spherulites showed mineralized bacteria (Figure 9d,f) and nanoparticles as observed in the earliest precipitation (Figure 7e). EDX spectra of the bioliths indicate C, O, Ca^{+2} and Mg^{+2} with minor amount of P. The P content significantly decreased throughout the incubation time in contrast to Mg^{+2} content. With increasing incubation time, the bioliths with different sizes containing various amounts of Ca and Mg carbonates were formed. Unlike Ca^{+2} bearing bioliths, Mg^{+2} bearing ones were commonly observed at the end of the incubation time (37 days).

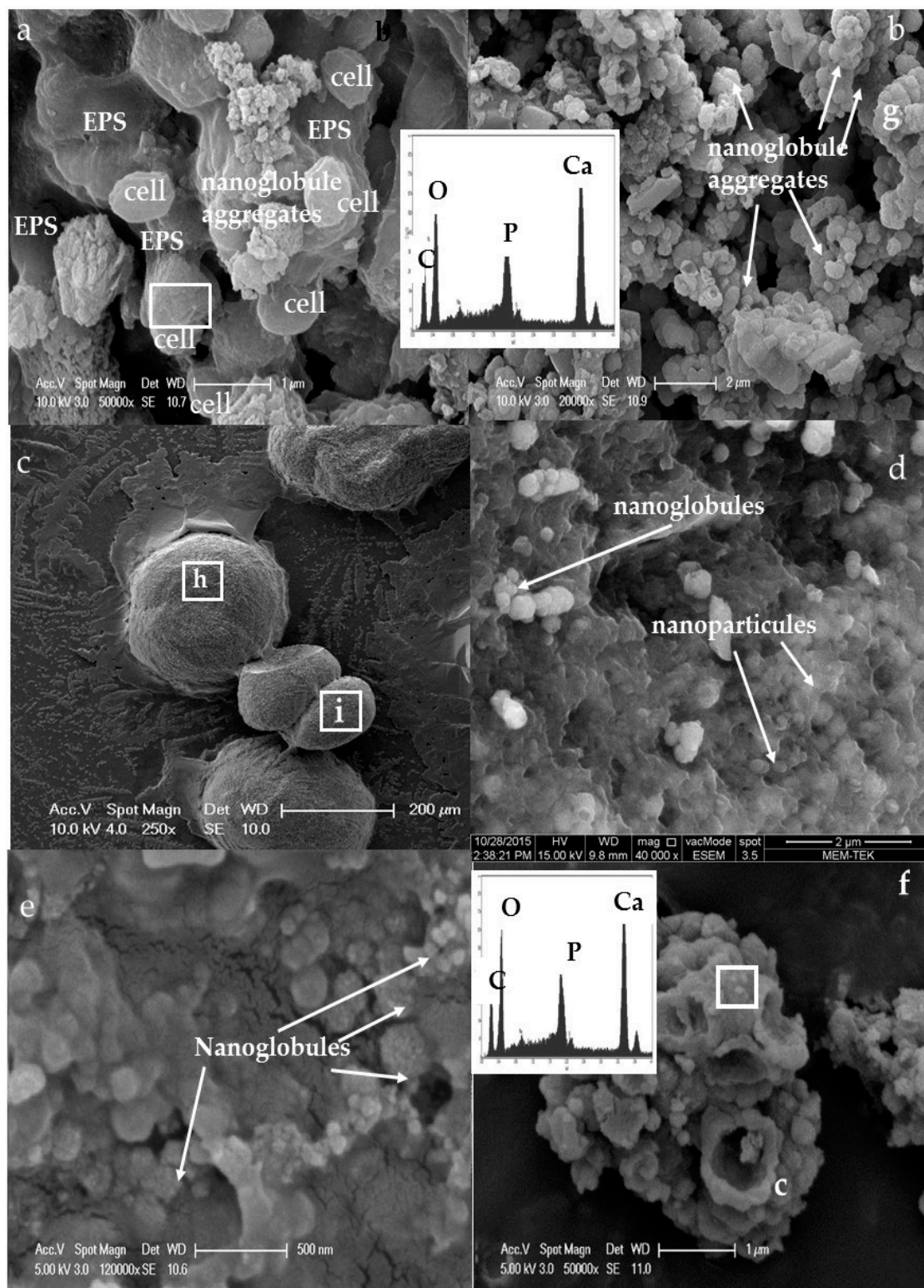


Figure 8. SEM photomicrographs and EDX spectra of carbonate bioliths formed during 10 days of incubation: (a) calcite with spiny surfaces and nanoglobule aggregates closely associated with EPS and the cells (M6 experiment); note the early stage of calcite crystal associated with the cell in the area squared; (b) nanoglobule aggregates with EDX (g); (c) spherulite and dumbbell (M6 experiment); (d) a closer view of the area h square in c, note the aggregated nanoparticles on the surface of calcite (M6 experiment); (e) a closer view of the area i square in c, note irregular size of nanoglobules on the surface of spherulite (i) in c; and (f) aggregated nanoglobules and mineralized bacteria with EDX spectra of the squared area.

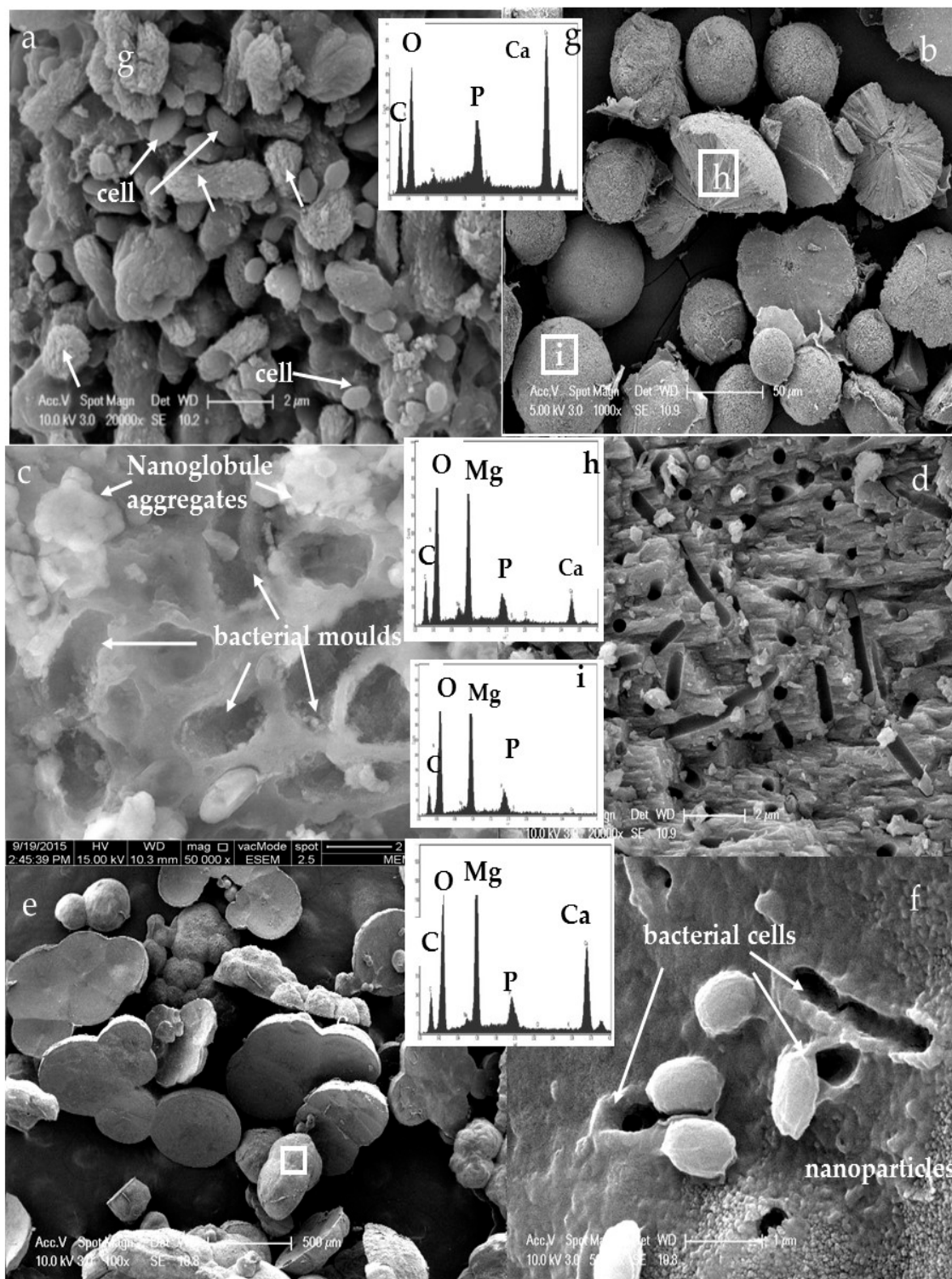


Figure 9. SEM photomicrographs of carbonate bioliths at the end of the experiments (37 days of incubation): (a) Calcite crystal (arrow indicate), drusiform calcite (g) formed accumulation of nanocrystals calcite with EDX in M3 experiment; (b) Isolated spherical bioliths. In square h hydromagnesite with fibrous radiated internal structure with EDX (i) (M8 experiment) and spheroidal hydromagnesite in square I; (c) A closer view of the area i square in b, note the nanoglobules around bacterial moulds (M7 experiment); (d) A closer view of the area h square in b, interior of fibrous radiated spherulite with reticulated zones and widespread bacterial moulds (M8 experiment); (e) Large spherulites and dumbbell shape bioliths (M6 experiment); (f) A closer view of the square area in e with EDX, surface of spherulite and the bacterial moulds is formed by aggregates of crystalline nanoparticles.

4. Discussion

4.1. Bacterial Nucleation and Carbonate Precipitation

A mix natural halophilic population used in the current study promoted precipitation of carbonate and phosphate nanoglobules at the early stage of carbonate precipitation (3–5 days) under various geochemical conditions (Figure 6). The nanoglobules are intimately associated with the cell surface, often embedded in organic films (e.g., EPS), and occur in the outer side of bacterial surface (Figure 6a–f). In fact, in some cases the cell surface of bacteria is no longer visible due to the abundance of nanoglobules (Figure 6b,c). Spheroidal, dumbbells and ovoidal shape carbonates are formed later with the extend of incubation (Table 2, Figure 8a,d,e and Figure 9c,e). Systematic presence of P on surface of carbonate bioliths throughout the incubation time suggest evolvement of nanoglobules into various carbonates depending on the chemical composition of precipitation solution (Figure 8a,b,e,f and Figure 9b–f). Consistently, observation of mineralized bacteria delimiting by nanoparticles on the surface of spherulites (Figure 9f) and nanoglobules around bacterial molds (Figure 9c) further support this.

Consistent with our results, formations of nanoglobules and nanoparticles have been reported for Ca and/or Mg carbonates [14,21,22] and for Fe carbonates and phosphates in culture experiments with different pure strains [33,34]. Demonstrating of formation of nanoglobules by a mix natural heterotrophic population together with the previous studies indicate that formation of nanoglobules and nanoparticles may not be specific to a microbial strain or activity of a particular microbial group as suggested earlier by Sanchez et al. [34]. Particularly, lack of precipitation in the control experiments (abiotic and with dead bacterial cells) confirm that active metabolism of halophilic bacteria is essential to induce formation of various carbonate minerals. Saturation index values (>0 or close to 0) calculated for the initial conditions of all the media indicate physico-chemical conditions that favor chemical precipitation of aragonite, calcite and dolomite in the M1 and M2 medium, dolomite in M4, M6, M7, and M8, and, particularly, hydroxyapatite in all the media assayed (Table 4). Absence of precipitation in the control flasks throughout the experiments imply that although saturated condition occurs with respect to a particular mineral phase(s) abiotic precipitation may not form due to a kinetic barrier (e.g., activation energy barrier) [35,36]. Additionally, since these experiments were conducted at ambient temperature, no precipitation of dolomite should be expected since dolomite requires high temperature (>100 °C) and supersaturation to form in purely chemical systems. These results further emphasis that solid phases were only formed in the presence of halophilic bacteria.

Table 4. Initial saturation index values of different minerals in the experimental media at 30 °C.

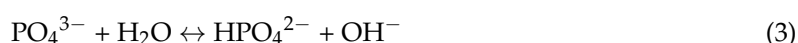
Mineral Phase	M1	M2	M3	M4	M6	M7	M8
Aragonite	0.38	0.57	−1.9	0.34	0.06	−0.56	−0.02
Calcite	0.52	0.71	−1.76	−0.48	−0.23	−0.39	0.15
Dolomite(disordered)	0.02	0.03	−0.32	−0.37	1.07	0.87	1.11
Halite	−1.65	−0.96	−4.58	−0.96	−1.36	−0.34	−1.35
Huntite	−4.65	−3.71	−11.45	−1.42	0.01	−0.65	0.3
Hydromagnesite	−15.75	−14.63	−21.96	−10.05	−7.27	−4.96	−6.57
Hydroxyapatite	14.23	14.9	1.51	14.42	11.43	8.45	11.23
Magnesite	−0.87	−0.63	−0.48	−0.60	0.07	0.49	0.19
Monohydrocalcite	−0.44	−0.56	−0.68	−0.98	−1.19	−1.24	−1.14
Nesquehonite	−3.36	−3.19	−4.8	−2.35	−2.66	−2.32	−2.54
Struvite	−0.05	0.05	−0.42	−0.36	−0.56	−0.61	−0.74

Aerobic heterotrophic bacteria like those used in the current experiments can induce mineral precipitation by creating supersaturated microenvironments surrounding their cell surfaces. By metabolizing organic substrates (e.g., glucose, peptone, yeast, amino acids) used in the medium they cause production of CO₂, NH₃ and PO₄^{3−} [13,14,37]. Bacterial emission of CO₂ produced during

metabolization of organic compounds cause acidifying effect on the system and lowers the carbonate saturation state (Equation (1)).



In fact, initial pH drop accompanying increase in the concentration of Ca^{+2} and Mg^{+2} at the beginning of the experiments further support pH decrease as a result of acidifying effect of glucose metabolization as shown by Rivadeneyra et al. [14] (Figures 2 and 3). Nevertheless, increase in the pH (from 7.2 to 9) counteracts this effect and provide alkalinity necessary for carbonate precipitation via Equations (2)–(5) (Figure 2). The pH rise occurs due to: (1) protonation of NH_3 and PO_4^{3-} ions released by metabolizing organic compounds to NH_4^+ and HPO_4^{2-} (Equations (2) and (3)); and (2) CO_2 outgassing from the experiments as a results of nature of aerobic experiments.



H^+ consumption cause shifting the carbonate equilibrium towards CO_3^{2-} (Equations (4) and (5)), thereby increasing the saturation state of carbonate minerals. Bacterial cell surface often negatively charged such as those in our experiments can catalyze precipitation by adsorbing cations (e.g., Ca^{+2} , and Mg^{+2}) on the cell surface or cell wall where the minerals nucleate. In such situation bacteria act as a catalyzer by overcoming a kinetic barrier (e.g., lowering activation energy) preventing the precipitation of a mineral in a supersaturated solution [38]. Morphologies of spherulites observed in the experiments further support that precipitation occurred in the supersaturated conditions via spherulitic growth (Figure 8c,d and Figure 9b) [39–42].

Spherulitic growth and its mechanism has been reported in various systems (e.g., biotic, and abiotic) [39–44]. Spherulitic growth of a material can occur via a nucleation controlled growth process with a continuous nucleation of new particles on the surface of existing particles [39]. This process is called as “growth front nucleation” and results in formation of spherulites with various morphologies and size consisting of aggregated nanoparticles as observed in the current experiments [39,40,43]. (Figure 9b,f). In addition to the nucleation site, high supersaturation conditions are considered prerequisite for the continuous growth front nucleation process. Presence of aggregates of crystalline nanoparticles and bacterial molds on the surface of spherulites may indicate a growth front nucleation process in the experiments. It is clear that bacteria create conditions to favor precipitation of the minerals via spherulitic growth by providing nucleation site and creating continues supersaturated conditions in their microenvironments during their metabolic activities. Consistently, demonstrating precipitation of spherulitic dolomite in various culture experiments at ambient temperature suggest that a spherulitic growth mechanism can be considered to be the controlling prerequisite for the formation of the intricately shaped biomineralized dolomite in modern hypersaline settings [4,7,17,22,43–45].

The metabolic activity of the halophilic culture supplies the ions necessary for the precipitation of minerals, phosphate ions for phosphate minerals, and carbonate ions for carbonates. In addition, they create appropriate microenvironments around the cell surface and provide nucleation site for adsorption of ions and initial formation of nanoglobules as it has been observed for the other microorganisms [14,20–22,33,37]. Several biologic macromolecules such as phospholipids and proteins as well as EPS have been reported as a potential nucleation site for adsorption of Ca^{+2} [33,34,37,46,47]. Observation of nanoglobules particularly rich in P or in close spatial association to cell surface and EPS indicate the role of an organic matrix rich in phosphate group for the initial nucleation of carbonate and phosphate rich nanoglobules. The nanoglobules attached to the cell wall or cell surface and observation of mineralized bacteria with carbonate minerals suggest that attachment of Ca^{+2} and Mg^{+2}

to the surface of bacteria followed by formation of nanoglobules may be a common initial step for microbial carbonate formation under hypersaline conditions.

4.2. Influence of Salinity and Mg^{+2}/Ca^{+2} Ratios on Bacterial Nanoglobule Formation

Different microbial species have been used in the laboratory and field based studies to elucidate microbial carbonate precipitation mechanisms (Table 5). We discuss our results in the context of several recent culture-based studies (both biotic and abiotic) compiled in Table 5. The mix halophilic culture cause formation of nanoglobules at various Mg^{+2}/Ca^{+2} ratios and further precipitated varying amounts of Ca^{+2} and/or Mg^{+2} carbonate minerals in all the salt concentrations tested except M1 and M2 experiments. The precipitation of similar nanoglobules to ours was reported in different laboratory experiments with different pure strains [7,14,21,22,46,47] in addition to natural settings where microbial carbonate precipitation take place [17,18,25,48–50]. By using similar Mg^{+2}/Ca^{+2} ratio (6.2) to ours (Mg^{+2}/Ca^{+2} ratio 7.2), Alois et al. [21] demonstrated formation of carbonate nanoglobules even under anoxic condition (Table 5). Under different experimental conditions than ours (e.g., medium components, pH, salinity), Sánchez-Román et al. [22] reported formation of nanometer scale dolomite in the experiments inoculated by the similar species to our culture experiments (*Virgibacillus marismortui* AJ00979 and *Halomonas meridiana*). The most striking example of formation of nanoglobules was reported by Sánchez-Román et al. [33]. The author showed siderite (Fe-carbonate) nanoglobules mediated by iron reducing bacterium under extreme acidic conditions. Benzerara et al. [46] reported nanometer-sized poorly crystalized calcium phosphate and crystalized nanocrystalline hydroxyapatite formation with a β -proteobacterium strain *Ramlibacter tataouinensis* isolated from the arid environments. Although we used different experimental conditions, mix heterotrophic halophilic bacteria in our experiments created conditions for formation of nanoglobules under various Mg^{+2}/Ca^{+2} ratios (Figures 6 and 8).

At Mg^{+2}/Ca^{+2} 0.1 ratio chlorapatite was the only mineral identified Like struvite, rarely observed in nature, chlorapatite appears to be an artifact of the liquid culture experiments containing large amounts of nitrogenous compounds, phosphate and calcium in M1 and M2 experiments (Figure 10). The precipitation amount was always higher in 80 g/L salinity experiments where the highest consumption of organic compounds was measured (Figure 4). Wide spread nanoglobule formation was particularly evident in M6 medium (Mg^{+2}/Ca^{+2} ratio 7.2 and 80 g/L salinity) where the highest percentage of calcite was identified as a carbonate mineral (Table 3). EDX spectra of the nanoglobules indicate Ca^{+2} enrichment even at high Mg^{+2}/Ca^{+2} ratio experiments (Figure 7A,B). This seems consistent with the previous studies which demonstrated that Ca^{+2} ion is more frequently adsorbed to bacterial surface compared to Mg^{+2} and bacterial Ca^{+2} pump is located near the outside of the cell, whereas the Mg^{+2} pump is located towards the inside and thereby extracellular Ca^{+2} concentration is much higher than the intracellular Ca^{+2} [11–15]. This selective enrichment should create conditions in the microenvironments of the bacterial cell surface to precipitate Ca^{+2} containing phases as in the case of the current study. Despite the fact that the same mix culture was used for each experimental condition, different percentage of minerals were formed in various experiments (Table 3). With increasing salinity and at nearly same Mg^{+2}/Ca^{+2} ratio (M6, M7 experiments) hydromagnesite was favored. Consistent with our results, diagenetic formation of Mg carbonates (e.g., huntite and hydromagnesite) has been reported in mud-flat lacustrine dolomites related to arid or semi-arid conditions in addition to in brine soaked mud-flats of lakes and their origin were attributed to halophilic bacterial mediation [9,28]. In summary, in contrast to different microbial species (e.g., sulfate and iron reducer, and aerobic heterotrophs), formation of bacterial nanoglobules intimately associated with the cell surfaces are reported under various experimental conditions (e.g., Mg^{+2}/Ca^{+2} ratio, temperature, and salinity) suggesting that while formation of nanoglobules may not be restricted to a specific microbial metabolism, the mineralogical composition of these structures would be influenced by ionic composition of precipitation solution. Reporting nanoglobules from natural environments with different physicochemical characters seems to be consistent with this [25,26,33,51].

Table 5. Compilation of previous studies reported formation of nanoglobules under various experimental conditions.

Experiment	Media Composition									Microbial Strains			Nanoglobules	Precipitated Minerals		
	Ca ⁺² mmol/L	Mg ⁺² mmol/L	Mg ⁺² /Ca ⁺² mmol/L	Na ⁺ mmol/L	K ⁺ mmol/L	SO ₄ ²⁻ mmol/L	PO ₄ ³⁻ mmol/L	Salt (%)	pH	T (°C)	Oxic/anoxic	Liquid			Agar	
Current Study	M1	23	2	0.1				8	7.2	30	O	X	X	<i>Halomonas saccharovitans</i> strain AJ275	No	Capatite
	M2	23	2	0.1				15	7.2	30	O	X	X	<i>Idiomarina</i> sp. TBZ29, 98%	No	Capatite
	M3	13	13	1				8	7.2	30	O	X	X	<i>Virgibacillus marismortui</i> <i>Bacillus selenitireducens</i> strain M1S6-17	Yes	Aragonite, Calcite, Dolomite, Struvite
	M4	13	13	1				15	7.2	30	O	X		<i>Halomonas saccharovitans</i> strain AJ275	Yes	Calcite, Dolomite, Struvite
	M5*	10	40	4				8	7.2	10	O	X		<i>Salinicoccus roseus</i> strain DSM 5351	no data	no data
	M6	5	36	7.2				8	7.2	30	O	X	X	<i>Halomonas alimentaria</i> strain L7B	Yes	Calcite, Dolomite, Monohydrocalcite, Struvite
	M7	5	36	7.2				15	7.2	30	O	X	X	<i>Planococcus maritimus</i> isolate LLQ	Yes	Calcite, Dolomite, Hydromagnesite, Struvite
	M8	5	56	11.2				8	7.2	30	O	X	X	<i>Planococcus rifietoensis</i> strain M8	Yes	Magnesian Calcite, Dolomite Hydromagnesite, Struvite
Krause et al. [48]	10	54	5	470	10	28		35		21	A	X		<i>Desulfobulbus mediterraneus</i>	Yes	Dolomite
Sánchez-Román et al. [34]								0.25	6.0	30	A	X		<i>Tessaracoccuslapidicaptus</i> CECT8385	Yes	Siderite and Vivianite
Sánchez-Román et al. [33]									3.5	35	A	X	X	<i>Acidiphilium</i> sp. PM	Yes	Siderite
Sánchez-Román et al. [22]									7.2	25-35	O		X	<i>Halomonas meridiana</i> ACAM 246 <i>Virgibacillus marismortui</i> AJ009793	Yes	Dolomite, Hydromagnesite
Alois et al. [21]	13 0	80 0.49	6.2 0.49	737 312	7.2 7.2	10 35.2	0.9 1.6	8 8	30 30		A A	X X		<i>Desulfonatronum lacustre</i> <i>Desulfonatronum lacustre</i>	Yes No	Calcite
Roberts et al. [25]	3.71	1.34	0.43	0.3	0.3	0.01			6.9		A	X		<i>Methanogenic species</i>	Yes	Dolomite
Benzerara et al. [46]	3.63									30	O		X	<i>Ramlibacter tataouinensis</i> , a B-proteobacterium	Yes	Calcium phosphate
Warthmann et al. [18]						10			8.0		O			SRB LVform6 <i>Desulfonatronovibrio</i> <i>hydrogenovorans</i>	Yes	Dolomite
Vasconcelos et al. [17]			Lagoa Vermelha natural sediment incubation						8	30		A	X	<i>Desulfovibrio</i> group	Yes	Dolomite

* no bacterail growth; O: oxic; A: anoxic; X: applied.

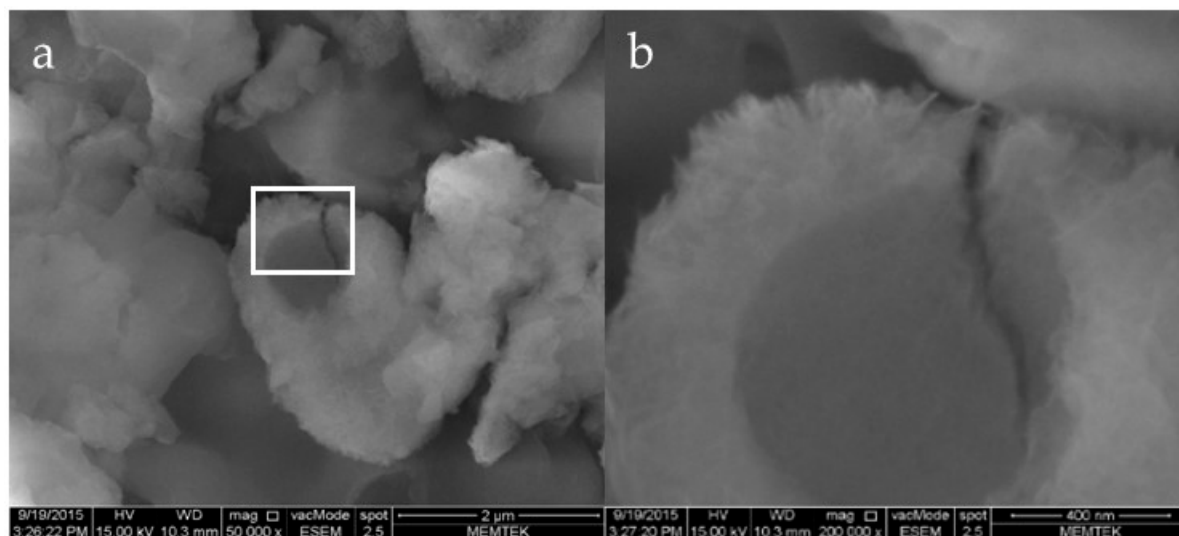


Figure 10. (a) Apatite crystal developed in M1 and M2 experiments; and (b) a closer view of the squared area in a.

5. Conclusions

We reported for the first time nanoscale microbial carbonate precipitation with a mixed natural halophilic culture enriched from hypersaline lake sediments. Nanoglobules formed closely associated with the cell surfaces of mix halophilic culture under various physicochemical conditions (e.g., salinity, and Mg^{+2}/Ca^{+2} ratios). In general, Ca content of nanoglobules was significantly higher compared to its Mg content, even at high Mg^{+2}/Ca^{+2} ratio (8). Consistently, extensive formation of Ca^{+2} containing carbonates (e.g., calcite) took place in the close vicinity of the cell surfaces in contrast to Mg rich carbonates (e.g., hydromagnesite). Formation of similar nanoglobules in other culture experiments and natural settings where microbial carbonates occur suggest that microbial carbonate nucleation may be an important early step during microbially mediated carbonate precipitation. Although saturated conditions formed with respect to particular mineral phase(s), lack of precipitation in abiotic experiments further indicates necessity of metabolic activity for precipitation. Our experimental results also emphasize that formation of nanoglobules may not be restricted to a single microbial group and their chemistry most likely results from interplay of ionic composition of chemical environment (e.g., Mg^{+2}/Ca^{+2} ratio) and microbial effects. Overall, the current study provides potential biogeochemical signatures (e.g., nanoscale carbonate) that can be used to trace microbial activity similar to aerobic halophiles in carbonate precipitation environments in geochemically diverse settings (e.g., Mg^{+2}/Ca^{+2} ratios).

Acknowledgments: We are grateful to Mehmet Seref Sonmez for his assistance with Rietveld method and XRD analysis and Nevin Karaguler for her guidance on PCR studies. We extend our gratitude to Patrick Meister and A.H. Gultekin for stimulating and valuable discussion during the project. This work was supported by Istanbul Technical University Research Division (ITU-BAP) grant to N. BALCI (39768) and TUBITAK (the Scientific and Technological Research Council of Turkey) grant to N. BALCI (113Y464).

Author Contributions: Nurgul Balci wrote the manuscript and contributed to the field and laboratory work as well as analyzed the data. Cansu Demirel carried out the experiments and contributed to the field and laboratory work in addition to writing the manuscript.

Conflicts of Interest: The authors declare that they have no conflict of interest.

References

1. Kastner, M. Control of dolomite formation. *Nature* **1984**, *311*, 410–411. [[CrossRef](#)]

2. Ferrer, M.R.; Quevedo-Sarmiento, J.; Rivadeneyra, M.A.; Béjar, V.; Delgado, R.; Ramos-Cormenzana, A. Calcium carbonate precipitation by two groups of moderately halophilic microorganisms at different temperatures and salts concentrations. *Curr. Microbiol.* **1988**, *17*, 221–227. [[CrossRef](#)]
3. Castanier, S.; Me'tayer-Levrel, G.L.; Perthuisot, J.-P. Ca-carbonates precipitation and limestone genesis—The microbiologist point of view. *Sediment. Geol.* **1999**, *126*, 9–23. [[CrossRef](#)]
4. Váscnelos, C.; McKenzie, J.A. Microbial mediation of modern dolomite precipitation and diagenesis under anoxic conditions (Lagoa Vermelha, Rio de Janeiro, Brazil). *J. Sediment. Res.* **1997**, *67*, 378–390.
5. Van Lith, Y.; Warthmann, R.; Vasconcelos, C.; McKenzie, J.A. Microbial fossilization in carbonate sediments: A result of the bacterial surface involvement in carbonate precipitation. *Sedimentology* **2003**, *50*, 237–245. [[CrossRef](#)]
6. Sánchez-Román, M.; McKenzie, J.A.; de Luca Rebello, W.A.; Rivadeneyra, M.A.; Váscnelos, C. Presence of sulfate does not inhibit low-temperature dolomite precipitation. *Earth Planet. Sci. Lett.* **2009**, *285*, 131–139. [[CrossRef](#)]
7. Sánchez-Román, M.; Romanek, C.S.; Fernández-Remolar, D.C.; Sánchez-Navas, A.; McKenzie, J.A.; Pibernat, R.A.; Váscnelos, C. Aerobic biomineralization of Mg-rich carbonates: Implications for natural environments. *Chem. Geol.* **2011**, *281*, 143–150. [[CrossRef](#)]
8. Ehrlich, H.L. *Geomicrobiology: Fifth Edition*; CRC Press Taylor & Francis Group: Boca Raton, FL, USA, 2009; p. 589.
9. Balci, N.; Menekşe, M.; Karagüler, N.; Sönmez, M.Ş.; Meister, P. Reproducing Authigenic Carbonate Precipitation in the Hypersaline Lake Acıgöl (Turkey) with Microbial Cultures. *Geomicrobiol. J.* **2016**. [[CrossRef](#)]
10. Balci, N.C. Effect of bacterial activity on trace metals release from oxidation of sphalerite at low pH (<3) and implications for AMD environment. *Environ. Earth Sci.* **2010**, *60*, 485–493.
11. Rivadeneyra, M.A.; Delgado, G.; Ramos-Cormenzana, A.; Delgado, R. Precipitation of carbonates by *Deleya halophila* in liquid media: Pedological implications in saline soils. *Arid Soil Res. Rehabil.* **1997**, *11*, 35–49. [[CrossRef](#)]
12. Rivadeneyra, M.A.; Delgado, G.; Ramos-Cormenzana, A.; Delgado, R. Biomineralization of carbonates by *Halomonas eurihalina* in solid and liquid media with different salinities: Crystal formation sequence. *Res. Microbiol.* **1998**, *149*, 277–286. [[CrossRef](#)]
13. Rivadeneyra, M.A.; Paraga, J.; Delgado, G.; Ramos-Coormenzana, A.; Delgado, G. Biomineralization of carbonates by *Halobacillus trueperi* in solid and liquid media with different salinities. *FEMS Microbiol. Ecol.* **2004**, *48*, 39–46. [[CrossRef](#)] [[PubMed](#)]
14. Rivadeneyra, M.A.; Martín-Algarra, A.; Sánchez-Román, M.; Sánchez-Navas, A.; Martín-Ramos, D. Amorphous Ca phosphate precursors for Ca-carbonate biominerals mediated by *Chromohalobacter marismortui*. *ISME J.* **2010**, *4*, 922–932. [[CrossRef](#)] [[PubMed](#)]
15. Rivadeneyra, M.A.; Martín-Algarra, A.; Sánchez-Navas, A.; Martín-Ramos, D. Carbonate and phosphate precipitation by *Chromohalobacter marismortui*. *Geomicrobiol. J.* **2006**, *23*, 1–13. [[CrossRef](#)]
16. Bosak, T.; Newman, D.K. Microbial nucleation of calcium carbonate in the Precambrian. *Geology* **2003**, *31*, 577–580. [[CrossRef](#)]
17. Vasconcelos, C.; McKenzie, J.A.; Bernasconi, S.; Grujic, D.; Tien, A.J. Microbial mediation as a possible mechanism for natural dolomite formation at low temperatures. *Nature* **1995**, *377*, 220–222. [[CrossRef](#)]
18. Warthmann, R.; van Lith, Y.; Váscnelos, C.; McKenzie, J.A.; Karpoff, A.M. Bacterially induced dolomite precipitation in anoxic culture experiments. *Geology* **2000**, *28*, 1091–1094. [[CrossRef](#)]
19. Sánchez-Román, M.; Rivadeneyra, M.A.; Váscnelos, C.; McKenzie, J.A. Carbonate and phosphate precipitation by halophilic bacteria: Influence of Ca and Mg ions. *FEMS Microbiol. Ecol.* **2007**, *6*, 273–284. [[CrossRef](#)] [[PubMed](#)]
20. Bontognali, T.R.R.; Vasconcelos, C.; Warthmann, R.; Dupraz, C.; Bernasconi, S.M.; McKenzie, J.A. Microbes produce nanobacteria-like structures, avoiding cell entombment. *Geology* **2008**, *36*, 663–666. [[CrossRef](#)]
21. Aloisi, G.; Gloter, A.; Krüger, M.; Wallmann, K.; Guyot, F.; Zuddas, P. Nucleation of calcium carbonate on bacterial nanoglobules. *Geology* **2006**, *34*, 1017–1020. [[CrossRef](#)]
22. Sanchez-Roman, M.; Vasconcelos, C.; Schmid, T.; Dittrich, M.; McKenzie, J.A.; Zenobi, R. Aerobic microbial dolomite at the nanometer scale: Implications for the geologic record. *Geology* **2008**, *36*, 879–882. [[CrossRef](#)]

23. Bundeleva, I.A.; Shirokova, L.; Pokrovsky, O.S.; Bénézeth, P.; Ménez, B.; Gérard, E.; Balor, S. Experimental modeling of calcium carbonate precipitation by cyanobacterium *Gloeocapsa* sp. *Chem. Geol.* **2014**, *374*, 374–375, 44–60. [[CrossRef](#)]
24. Bundeleva, I.A.; Shirokova, L.; Bénézeth, P.; Pokrovsky, O.S.; Kompantseva, E.I.; Balor, S. Calcium carbonate precipitation by anoxygenic phototrophic bacteria. *Chem. Geol.* **2012**, *291*, 116–131. [[CrossRef](#)]
25. Roberts, J.A.; Bennett, P.C.; Gonzáles, L.A.; Macpherson, G.L.; Milliken, K.L. Microbial precipitation of dolomite in methanogenic groundwater. *Geology* **2004**, *32*, 277–280. [[CrossRef](#)]
26. Kenward, P.A.; Goldstein, R.H.; Gonzalez, L.A.; Roberts, J.A. Precipitation of low-temperature dolomite from an anaerobic microbial consortium: The role of methanogenic Archaea. *Geobiology* **2009**, *7*, 556–565. [[CrossRef](#)] [[PubMed](#)]
27. Helvacı, C.; Alçiçek, C.; Gündoğan, İ.; Gemici, U. Tectonosedimentary Development and Palaeoenvironmental Changes in the Acıgöl Shallow-Perennial Playa-Lake Basin, SW Anatolia, Turkey. *Turkish J. Earth Sci.* **2012**, *21*, 1–20.
28. Mutlu, H.; Kadir, S.; Akbulut, A. Mineralogy and water chemistry of the Lake Acıgöl (Denizli), Turkey. *Carbonates Evaporites* **1999**, *14*, 91–99.
29. Schneegurt, M.A. Media and conditions for the growth of halophilic and halotolerant bacteria and archaea. In *Advances in Understanding the Biology of Halophilic Microorganisms*; Vreeland, R.H., Ed.; Springer: Dordrecht, The Netherlands, 2012; pp. 35–58.
30. Kuo, S. Phosphorus. In *Methods of Soil Analysis. Part 3: Chemical Methods*; Sparks, D.L., Page, A.L., Helmke, P.A., Loeppert, R.H., Eds.; Soil Science Society of America: Madison, WI, USA, 1996; pp. 894–895.
31. Hillier, S. Accurate quantitative analysis of clay and other minerals in sandstones by XRD: Comparison of a Rietveld and a reference intensity ratio (RIR) method and the importance of sample preparation. *Clay Miner.* **2000**, *35*, 291–302. [[CrossRef](#)]
32. Parkhurst, D.; Appelo, C.A.J. *User's Guide to PhreeqC (Version 2)—A Computer Program for Speciation, Batch-Reaction, One-Dimensional Transport, and Inverse Geochemical Calculations*; Water-Resources Investigations Report; 99-4259; U.S. Department of the Interior: Denver, CO, USA, 1999.
33. Sánchez-Román, M.; Fernández-Remolar, D.; Amils, R.; Sánchez-Navas, A.; Schmid, T.; San Martín-Uriz, P. Microbial mediated formation of Fe-carbonate minerals under extreme acidic conditions. *Sci. Rep.* **2014**, *4*, 4767–4776. [[CrossRef](#)] [[PubMed](#)]
34. Sánchez-Román, M.; Puente-Sánchez, F.; Parro, V.; Amils, R. Nucleation of Fe-rich phosphates and carbonates on microbial cells and exopolymeric substances. *Front. Microbiol.* **2015**. [[CrossRef](#)] [[PubMed](#)]
35. Morse, J.W. The kinetics of calcium carbonate dissolution and precipitation. In *Reviews in Mineralogy: Carbonates-Mineralogy and Chemistry*; Reeder, R.J., Ed.; Mineralogical Society of America: Chelse, MA, USA, 1983; pp. 227–264.
36. Moore, C.H. The nature of carbonate depositional systems-comparison of carbonates and silici clastics. In *Developments in Sedimentology*; Moore, C.H., Ed.; Elsevier: Amsterdam, The Netherlands, 1989; pp. 1–19.
37. Rivadeneyra, M.A.; Delgado, G.; Soriano, M.; Ramos-Cormenzana, A.; Delgado, R. Biomineralization of carbonates by *Marinococcus albus* and *Marinococcus halophilus* isolated from the Salar de Atacama (Chile). *Curr. Microbiol.* **1999**, *39*, 53–57. [[CrossRef](#)] [[PubMed](#)]
38. Konhauser, K.O. Diversity of bacterial iron mineralization. *Earth Sci. Rev.* **1998**, *43*, 91–121. [[CrossRef](#)]
39. Gránásy, L.; Pusztai, T.; Tegze, G.; Warren, J.A.; Douglas, J.F. Growth and form of spherulites. *Phys. Rev. Lett. E* **2005**, *72*, 011605. [[CrossRef](#)] [[PubMed](#)]
40. Andreassen, J.P.; Flaten, E.M.; Beck, R.; Lewis, A.E. Investigations of spherulitic growth in industrial crystallization. *Chem. Eng. Res. Des.* **2010**, *88*, 1163–1168. [[CrossRef](#)]
41. Bots, P.; Benning, L.G.; Rodriguez-Blanco, J.D.; Roncal-Herrero, T.; Shaw, S. Mechanistic Insights into the crystallization of amorphous calcium carbonate (ACC). *Cryst. Growth Des.* **2012**, *12*, 3806–3814. [[CrossRef](#)]
42. Sand, K.K.; Rodriguez-Blanco, J.D.; Makovicky, E.; Benning, L.G.; Stipp, S.L.S. Crystallization of CaCO₃ in water-alcohol mixtures: Spherulitic growth, polymorph stabilization and morphology change. *Cryst. Growth Des.* **2012**, *12*, 842–853. [[CrossRef](#)]
43. Rodriguez-Blanco, J.D.; Shaw, S.; Bots, P.; Roncal-Herrero, T.; Benning, L.G. The role of Mg in the crystallisation of monohydrocalcite. *Geochim. Cosmochim. Acta* **2014**, *127*, 204–220. [[CrossRef](#)]
44. Rodriguez-Blanco, J.D.; Shaw, S.; Benning, L.G. A route for the direct crystallization of dolomite. *Am. Mineral.* **2015**, *100*, 1172–1181. [[CrossRef](#)]

45. Cisar, J.O.; Xu, D.-Q.; Thompson, J.; Swaim, W.; Hu, L.; Kopecko, D.J. An alternative interpretation of nanobacteria-induced biomineralization. *Proc. Natl. Acad. Sci. USA* **2000**, *97*, 11511–11515. [[CrossRef](#)] [[PubMed](#)]
46. Benzerara, K.; Menguy, N.; Guyot, F.; Skouri, F.; de Luca, G.; Barakat, M.; Heulin, T. Biologically controlled precipitation of calcium phosphate by *Ramlibacter tataouinensis*. *Earth Planet. Sci. Lett.* **2004**, *228*, 439–449. [[CrossRef](#)]
47. Krause, S.; Liebetrau, V.; Goeb, S.; Sánchez-Román, M.; McKenzie, J.A.; Treude, T. Microbial nucleation of Mg-rich dolomite in exopolymeric substances under anoxic modern sea water salinity: New insight into an old enigma. *Geology* **2012**, *40*, 587–590. [[CrossRef](#)]
48. Folk, R.L. Nanobacteria and the precipitation of carbonates in unusual environments. *Sediment. Geol.* **1999**, *126*, 47–56. [[CrossRef](#)]
49. Folk, R.L.; Chafetz, H.S. Bacterially induced microscale and nanoscale carbonate precipitates. In *Microbial Sediments*; Riding, R.E., Awramik, S.M., Eds.; Springer: Berlin, Germany, 2000; pp. 40–49.
50. Dupraz, C.; Visscher, P.T.; Baumgartner, L.K.; Reid, R.P. Microbe–mineral interactions: Early carbonate precipitation in a hypersaline lake (Eleuthera Island, Bahamas). *Sedimentology* **2004**, *51*, 745–765. [[CrossRef](#)]
51. Benzerara, K.; Menguy, N.; López-García, P.; Yoon, T.; Kazmierczak, J.; Tyliszczak, T.; Guyot, F.; Brown, G.E. Nanoscale detection of organic signatures in carbonate microbiolites. *Proc. Natl. Acad. Sci. USA* **2006**, *103*, 9440–9445. [[CrossRef](#)] [[PubMed](#)]



© 2016 by the authors; licensee MDPI, Basel, Switzerland. This article is an open access article distributed under the terms and conditions of the Creative Commons Attribution (CC-BY) license (<http://creativecommons.org/licenses/by/4.0/>).